Astron. Astrophys. 342, 417–425 (1999)

ASTRONOMY AND ASTROPHYSICS

Fabry-Perot observations of the ionized gas in NGC 3938⋆

J. Jiménez-Vicente[1], **E. Battaner**[1], **M. Rozas**[2], **H. Castañeda**[2], **and C. Porcel**[1]

[1] Departamento de Física Teórica y del Cosmos, Universidad de Granada, E-18071 Granada, Spain
[2] Instituto de Astrofísica de Canarias, E-38200 La Laguna, Tenerife, Spain

Received 21 August 1998 / Accepted 12 November 1998

Abstract. The nearly face-on spiral galaxy NGC 3938 has been observed in the H_α line with the TAURUS II Fabry-Perot interferometer at the William Herschel Telescope in order to study the kinematics of the ionized gas. We are able to construct intensity, velocity and velocity dispersion maps for this galaxy. The rotation curve of the galaxy is calculated up to 4.5 radial scale lengths from the galactic centre. The residual velocity field shows very small values with no systematic pattern. The mean velocity dispersion is approximately constant with radius at about 11 km s^{-1} as previously reported for the neutral and molecular gas. We have also studied the relation between intensity and velocity dispersion for the ionized gas. We have found that this distribution is compatible with a turbulent gas relaxing to a Kolmogorov type turbulence as the stationary regime. The average dispersion varies with intensity as $\sigma \propto I^{1/8}$ although it becomes much steeper at higher intensities, for which the dispersion is kept almost constant at a value of about 19 km s^{-1}.

Key words: ISM: kinematics and dynamics – galaxies: individual: NGC 3938 – galaxies: ISM – galaxies: kinematics and dynamics – galaxies: spiral

1. Introduction

Kinematical studies of spiral galaxies are often performed by means of HI observations. This allows a study of the global kinematics (and gas distribution) throughout the whole galaxy up to very large radii, though it requires large observation times. As an alternative complementary technique, Fabry-Perot interferometry allows a very large amount of information to be extracted with quite short observation times. Although many studies should be carried out with the neutral atomic gas, Fabry-Perot interferometry may be a very good alternative if we are interested in the global kinematics of the galaxy. On the other hand, as we are observing a different emisson mechanism, differences in the deduced dynamical properties (i.e. in the neutral and ionized gas dynamics) may be a clue to understand some galactic kinematical features. We can extract standard information such as velocity maps, rotation curves, etc with very good spatial and spectral resolution.

In the case of face-on galaxies, Fabry-Perot interferometry is very adequate for the study of vertical motions. We can calculate residual velocity maps (which allow to study large scale vertical motions), velocity dispersions (whose knowledge is essential to understand the vertical equilibrium in the galaxy (see Combes & Bequaert, 1997)) etc. In particular it is specially well suited to study vertical motions over star forming regions which can be the key to understand disk-halo interactions according to some theoretical models (Norman & Ikeuchi, 1988). Even at larger scales, random motions, are strongly related with the magnetic difussivity in the disk, which could be a key ingredient in understanding the origin and structure of the galactic magnetic field.

Along this paper we extensively extract these kind of data for the galaxy NGC 3938. In Sect. 2 we review general properties of the galaxy. Sect. 3 is devoted to the observational procedure and data reduction. In Sect. 4 we discuss the distribution of the H_α emission. The kinematics is analysed in Sect. 5, including the rotation curve calculation and velocity dispersion analyses. The relation between intensity and velocity dispersion is studied in Sect. 6. The main results and conclusions are finally summarized in Sect. 7.

2. NGC 3938

NGC 3938 is a nearly face-on (inclination $\approx 14°$) late type (Sc) spiral galaxy (see Fig. 1[1]). Table 1 summarizes the main galaxy properties. It has quite well defined arms and is rich in HII regions. Its distance derived from its corrected radial velocity (848 km s^{-1} according to the RC3 catalog) is 11.3 Mpc (using a Hubble constant of 75 km/s/Mpc). At this distance, we have

⋆ Based on observations made with the William Herschel Telescope operated on the island of La Palma by the Isaac Newton Group in the Spanish Observatorio del Roque de los Muchachos of the Instituto de Astrofísica de Canarias

[1] Based on photographic data of the National Geographic Society – Palomar Observatory Sky Survey (NGS-POSS) obtained using the Oschin Telescope on Palomar Mountain. The NGS-POSS was funded by a grant from the National Geographic Society to the California Institute of Technology. The plates were processed into the present compressed digital form with their permission. The Digitized Sky Survey was produced at the Space Telescope Science Institute under US Government grant NAG W-2166.

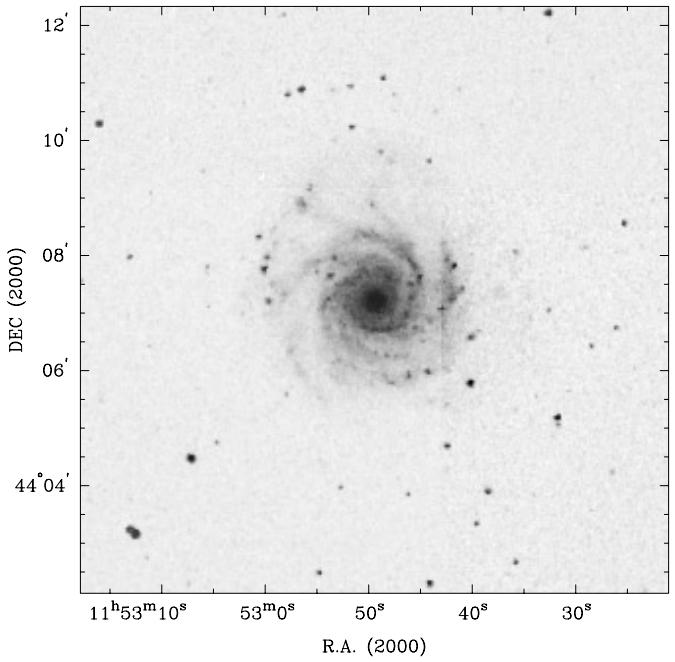

Fig. 1. Optical image of NGC 3938

54.78 pc/arcsec, or 61.36 pc/pixel, and therefore we are able to construct high resolution maps. The galaxy belongs to the Ursa Major Cluster (see Tully et al. 1996) but has no close companions within 100 kpc. Its radial scale length is 31.1 arcsec or 1.7 kpc (this value is for the K band as measured by Tully et al. 1996, although they found a clear trend to increase with decreasing wavelength). van der Kruit & Shostak (1982) carried out surface photometry of this galaxy in the F band and they fitted an exponential disc with a scale length of 36 arcsec, but they found a faster decline at $R \approx 2.5'$. It is approximately up to this point where our observations are able to reach.

The stellar velocity dispersion was measured by Bottema (1988). He stated that the central vertical stellar velocity dispersion is low with a value of about 30 km s^{-1}, and about 15 km s^{-1} at one radial scale length, compatible with an exponential decline as found in other galaxies (see Bottema (1993)), although he warns that in the outer region the values are below the resolution limit. For the bulge he found a velocity dispersion of about 40 km s^{-1}.

This galaxy has been observed in HI by van der Kruit & Shostak (1982) at Westerbork with a $24'' \times 36''$ beam. They found no systematic pattern of z-motions in excess of 5 km s^{-1}, although in a subsequent analysis of the residual velocity map by Foster & Nelson (1985) they found a ring and a spoke pattern. The velocity dispersion was observed to be constant with radius at a value of 10 km s^{-1}. CO observations with the IRAM 30-m telescope by Combes & Becquaert along the major and minor axis also found this behaviour for the molecular gas with a slightly smaller velocity dispersion of 8.5 km s^{-1}.

The HII region luminosity function has been calculated by McCall et al. (1996) by two methods (according to their nomenclature): Fixed Threshold Photometry (FTP) and Percentage of Peak Photometry (PPP). The luminosity function slope above the completeness limit (which they take $L_t = 38.9$ ergs s^{-1} and $L_t = 38.3$ ergs s^{-1} for each method respectively) is identical in both cases and its value is 1.7 ± 0.1. This value is within the range reported by Kennicutt et al. (1989) and Rozas et al. (1996) in other galaxies. It is worth noting that this completeness limit is quite high as compared with the values used by other authors such as Kennicutt et al. (1989) and Rozas et al. (1996). This value is much closer to the observed turnover in the luminosity function observed by Kennicutt et al. (1989) for galaxies of the same type and which he attributes to a transition between normal giant regions and supergiant regions. The same effect has been observed by Rozas et al. (1996) at a value of 38.6 ergs s^{-1}, and they explain this effect as a transition between ionization bounded and density bounded HII regions. If the completeness limit used by McCall et al. (1996) is taken as such a turnover, then the slope is low when compared with reported values for this range of the luminosity function in other galaxies.

Table 1. Galaxy properties

Name	NGC 3938
Type	Sc(s)I
R.A.(2000)	$11^h52^m49.8^s$
Dec (2000)	$44°07'26''$
B Magnitude	10.9
D_{25}	$5.4'$
$V_\odot$ (RC3)	809 km s^{-1}
V_{gsr} (RC3)	848 km s^{-1}
Distance	11.3 Mpc
Redshifted H_α	6580.5 Å
Inclination	$14°$
P.A.	$20°$
Environment	Ursa Major Cluster.
	No close (< 100 kpc) companions

3. Observations and data reduction

The observations were made on March 18, 1997, at the William Herschel Telescope. The night was not photometric and the seeing conditions were not very good with a measured seeing of 3 arcsec. This avoided photometric calibration of our data and therefore we will use arbitrary units for intensity throughout this paper. The galaxy was observed in the H_α line with the TAURUS II Fabry-Perot interferometer at the Cassegrain focus of the William Herschel Telescope. We used the $500\,\mu$ etalon and the f/2.11 camera with a TEK CCD detector. This setup gives a field of view of about 5 arcmin (because the interference filter at the focal plane is vignetting the field) and a pixel size of 0.56 arcsec. We rebinned 2x2 the CCD reading which results in a pixel size of 1.12 arcsec. The nominal spectral resolution of the etalon at 6500 Å is 9.75 km s^{-1} with a free spectral range of 195 km s^{-1}. We scanned the spectral range in 55 steps with an exposure time of 120 seconds each, giving a total of about 2 hours to take the full datacube. A calibration cube with a CuNe lamp was taken at the beginning of the night, and calibration

Table 2. Observational parameters

Date of observation	18/03/1997
Telescope	WHT
Focus	Cassegrain
Instrument	TAURUS II
Etalon	$500\,\mu$
Filter	6577/15
Detector	TEK CCD
Steps	55
Exposure time per step	120 sec
Free Spectral Range	194.1 km/sec
Instrumental width	7.7 km s^{-1}
Spectral resolution	3.61 km/sec/pixel
Pixel size	1.12 arcsec
Seeing	3 arcsec

rings were taken before and after the object exposure in order to make the phase calibration. The measured instrumental profile obtained after phase correcting the calibration datacube was 7.7 km s^{-1}, and the spectral resolution was 3.61 km/sec/pixel. Table 2 summarizes the observational setup.

The observed datacube is bias subtracted and phase corrected by standard procedures. We used the 6577/15 filter for order sorting. This filter allows the OH night sky line at 6577.28 Å to reach the etalon and therefore this spectrum is added to the target one. This effect should be corrected before the datacube is analysed. To do the correction, large regions of the observed field are chosen at places where there is no emission from the target and a spectrum is calculated for each of those regions. An average spectrum is calculated from all of them and an artificial datacube is created for a homogeneous source with that spectral content which is then subtracted from the original one.

We have also created lower resolution (12 arcsec) datacubes by smoothing the original one with a wider beamsize in order to have smoother maps as usually done with radio data. The rest of the data reduction procedure is the same as for the full resolution datacube, for which we briefly describe it below.

To extract the physical information from the phase corrected datacube we used the GIPSY package. First of all, we subtract the continuum from the full datacube using the velocity channels that have no H_α line emission, and then each spectrum is fitted to a gaussian function, from which we extract the velocity (line mean position), velocity dispersion (line width) and intensity (proportional to the line peak intensity) at each position. We have also used a standard moments procedure to calculate these maps. The velocity maps obtained by both methods match very well, but not so the dispersion map for which we prefer the gaussian fitting method. The reason to choose gaussian fitting instead of a moments procedure is to allow a better determination of velocity dispersions and avoid a systematic bias, as pointed out by van der Kruit & Shostak (1982).

The calculated maps are very noisy. To clean them we put constraints on the intensity and velocity dispersion selecting only those pixels for which these parameters exceed a certain

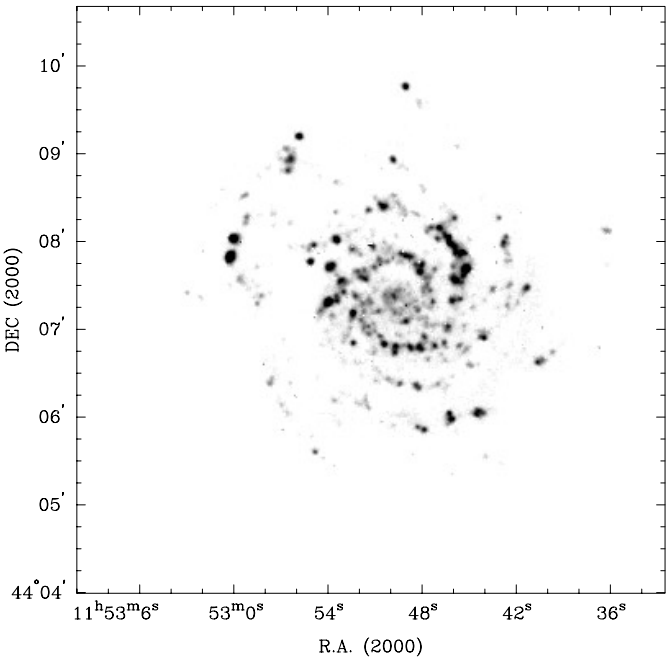

Fig. 2. Intensity map for NGC 3938

value. Finally, some remaining noise is eliminated by hand. The calculated velocity dispersion should be corrected because of the instrumental width (which is 7.7 km s^{-1}) and the natural line width (which is 3 km s^{-1} for the H_α line). These numbers should be quadratically subtracted from the measured dispersion. As we are mainly interested in calculating the non-thermal velocity dispersion, we should also correct for the thermal width. We have taken a typical temperature of $10^4\,K$ for the ionized gas (Spitzer, 1978 and Osterbrock, 1989). At this temperature the thermal width is 9.1 km s^{-1}.

Therefore we have, finally

$$\sigma_{nt} = (\sigma^2_{obs} - \sigma^2_{inst} - \sigma^2_{nat} - \sigma^2_{th})^{1/2} \quad (1)$$

where σ_{nt}, σ_{obs}, σ_{inst} and σ_{th} are the non-thermal, observed, instrumental and thermal components respectively.

4. The ionized gas distribution

The spatial distribution of the ionized gas can be seen in Fig. 2. Most of it comes from the HII regions but there is also emission coming from regions which cannot be clearly identified as HII regions. They can be low luminosity HII regions or belong to a *diffuse* component. Down to our detection level, most of this low intensity emission is seen in the periphery of HII regions. The HII regions are highly concentrated in the arms, mostly in the inner disc, but there are also giant HII regions at large galactocentric radii such as the two bright regions in the east. The northern arm is brighter than the southern one, and most of the bright HII regions are hosted by it. This will affect the global line profile as we will see later.

The radial distribution of the ionized gas can be seen in Fig. 3. It has been calculated by adding the intensity over rings with a width of 3.36 arcsec and dividing by the ring area. The

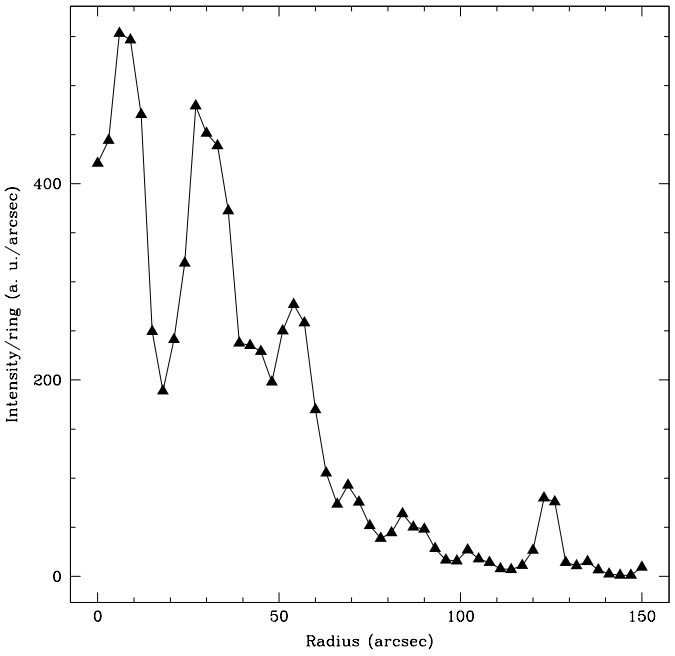

Fig. 3. Radial distribution of the ionized gas in NGC 3938

peaks at about 30 and 50 arcsec from the center are due to the spiral arms (especially at about 30 arcsec from the center, the spiral arms resemble a ring) and the peak at about 125 arcsec is due mainly to the pair of supergiant HII regions in the east.

5. Kinematics

The full resolution (1.12 arcsec/pixel) channel maps for the H_α line emission are shown in Fig. 4. Only each third channel is shown (with a separation of 10.83 km s^{-1} between them). Only the brightest emission regions are shown to avoid noise. A first inspection shows no special features but normal rotation and the absence of warping.

We have calculated the integrated H_α profile by summing the intensity in each channel. It is shown in Fig. 5. The profile does not show the usual double horn structure that can be seen in the HI profile for this galaxy in van der Kruit & Shostak (1982) and in other galaxies. This is partially due because the central part of the disc which is usually devoid of neutral atomic gas has now a quite large amount of emission. This is most often the case with H_α profiles and another clear example can be seen in Fig. 5 of Amram et al. (1996) with the galaxy DC 1842-63 n° 24. This region appears in channels close to the systemic velocity and therefore these channels show a larger flux than observed for the neutral gas as compared with the channels in the horns. On the other hand the profile asymmetry which can also be seen partially in the HI profile is due to the larger emission of the northern arm (as can be seen in Fig. 5) which is very rich in bright HII regions and which is in the receding part of the galaxy.

In the rest of this section we will study in detail the velocity and dispersion maps as well as the calculation of the rotation curve.

5.1. The velocity map

The velocity map at the highest available resolution (1.21 arcsec/pixel) is shown in Fig. 6 as calculated with the moments procedure. The global kinematics is better seen in the smoother map at 12 arcsec resolution shown in Fig. 7. It shows no special features but normal rotation although there are small traces of streaming motions near the inner arms. Anyway, these deviations from axisymmetric rotation are very small as we will see later. There are not traces of a warp as can be seen in the kinematical major axis which, is kept almost straight up to the largest radii. Our observations do not reach up to very large galactocentric radii and the warp could start further and be hidden to the present observations, but this is not very likely in this case as no warp has been observed in HI for which there are available data up to much larger radii.

5.2. Rotation curve

We have used the high resolution (1.12 arcsec/pix) velocity field using a tilted rings model fitting as described by Begeman (1989) using the ROTCUR task of the GIPSY package. The galaxy is divided into concentric rings and each of them is characterized by its inclination angle (i), position angle of the major axis (P.A.) and rotational velocity (V_c). In principle additional parameters can be fitted, such as the centre of each ring and its systemic velocity. These are too many parameters for a single fit and we preferred to calculate the latter at an earlier stage and then fix them in the final fitting procedure. Each data point in the velocity map is weighted by $|\cos(\theta)|$ where θ is the azimuthal angle measured from the major axis. Moreover, data with $|\theta < 5^\circ|$ are excluded from the fit.

The low inclination angle of NGC 3938 makes it difficult to fit simultaneously the rotational velocity and the inclination angle. As this galaxy shows no signs of a warp (see the velocity map in van der Kruit & Shostak (1982)) it is safe to use a constant inclination throughout the whole disc. We have chosen a value of $i = 14^\circ$. The effect of using a different angle but close to this value would be either to raise (if it were larger) or to lower (if it were smaller) the value of the rotational velocity, but its shape would remain unchanged.

As the number of data points in the outer part of the disk is very low, we have used wider rings in this region in order to keep a minimum number of pixels in each ring. The width of the rings has been calculated by demanding a minimum of 300 data points inside each ring. Therefore the outer parts of the fitted model are of poorer resolution, and so is the rotation curve.

The modeled velocity map for NGC 3938 is shown in Fig. 8. The rotation curve of the galaxy can be plotted with the calculated values for the rotational velocity of each ring and is shown in Fig. 9 with the fitted position angle of each ring.

This is the best determination of the rotation curve of NGC 3938 up to date. The value of the rotational velocity at large galactocentric radii agrees with previously published values at about $V_{rot} = 38 \csc i$ km s^{-1} (see van der Kruit & Shostak, 1982 and Combes & Becquaert, 1997), but our determination

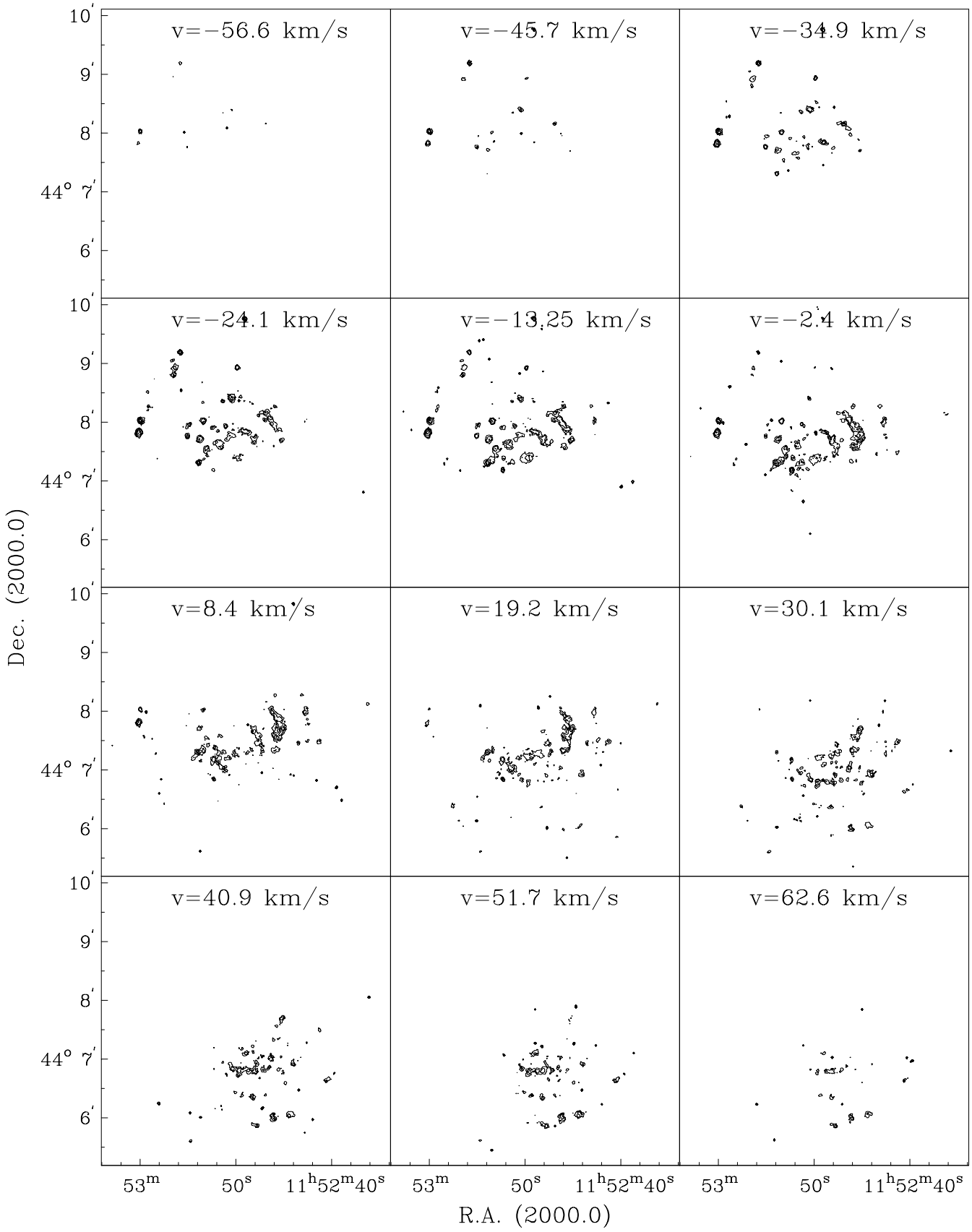

Fig. 4. Channel maps of the continuum subtracted H_α emission for NGC 3938 at 1.12 arcsec/pixel resolution. The velocity of each channel (with the systemic velocity of the galaxy subtracted) is shown at the *top* of each panel.

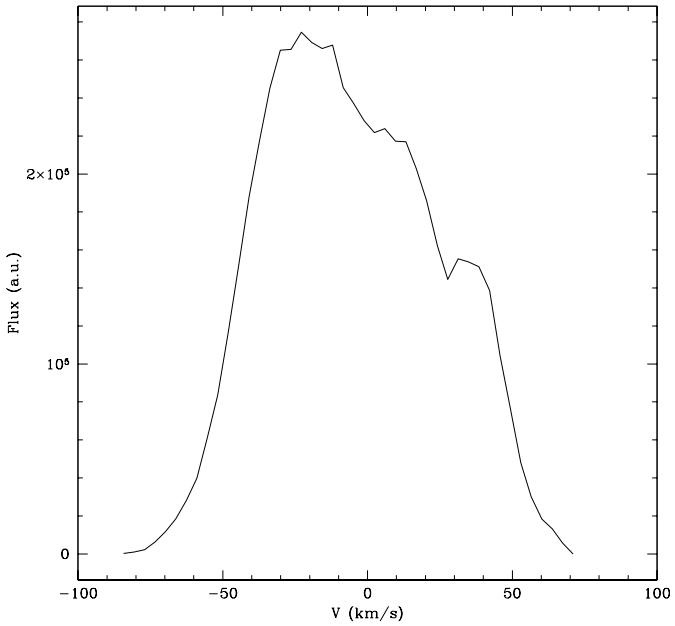

Fig. 5. Integrated H_α profile of NGC 3938

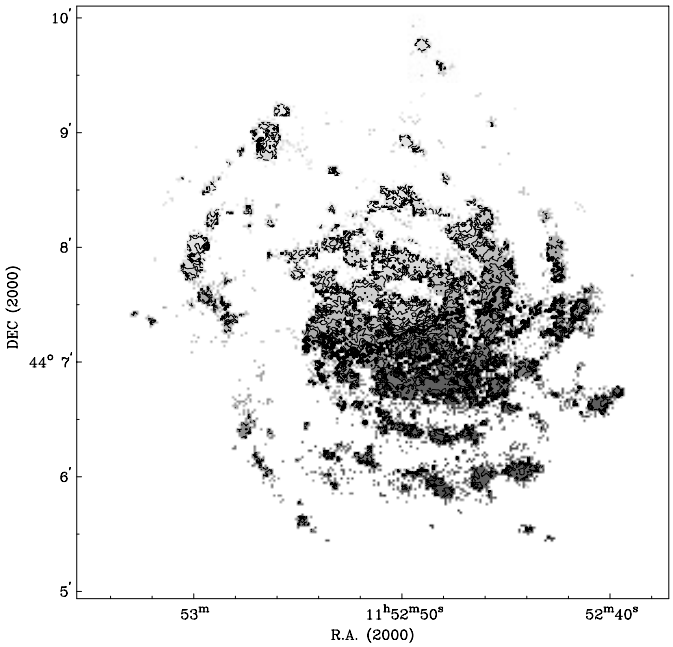

Fig. 6. High resolution (1.12 arcsec/pix) velocity map for NGC 3938. Levels are shown each 5 km s^{-1}. Dark gray shows the approaching region while light gray shows the receding region. The thick line shows the 0 km s^{-1} line.

of the curve has a much larger spatial resolution, especially at small radii. Bottema (1993) using the Tully-Fisher relation deduced a value of $V_{rot} = 147 \pm 20$ km s^{-1} (corresponding to an inclination of 15°) which is compatible with our determination of 157 km s^{-1}. At larger radii, the details of the shape of the rotation curve are not so reliable because of the small number of data points in the fit, but it gives the right value of the maximum rotational velocity if we assume it to be constant at large radii.

Fig. 10 shows a position-velocity diagram along the major axis with the inner part of the calculated rotation curve superimposed. It can be seen that the shape of the rotation curve matches very well the gas distribution.

5.3. The residual velocity map

The residual map at 12 arcsec resolution calculated by subtracting the fitted model velocity map from the observed map is shown in Fig. 11. The rms residual velocity calculated with the 12 arcsec resolution residual map is 4.6 km s^{-1}. We do not detect any systematic pattern in excess 10 km s^{-1} although some traces of the spiral arms can be seen in the inner parts. We have tried to compare this residual map with the one published by Foster & Nelson (1985). We find no similarities between them and although we have not repeated their logarithmic spiral decomposition it is not very likely that the ring and the spoke are detectable in our map.

Some regions with a noticeable residual velocity seem to be associated with bright HII regions with very high velocity dispersions.This is, for instance, the case for the northward one in the pair of regions in the furthest east which shows a systematic defect of about 10 km s^{-1}. There is no clear evidence that this residual is a true movement of these regions but the coincidence is worth being noted. Phenomena such as the chimneys proposed

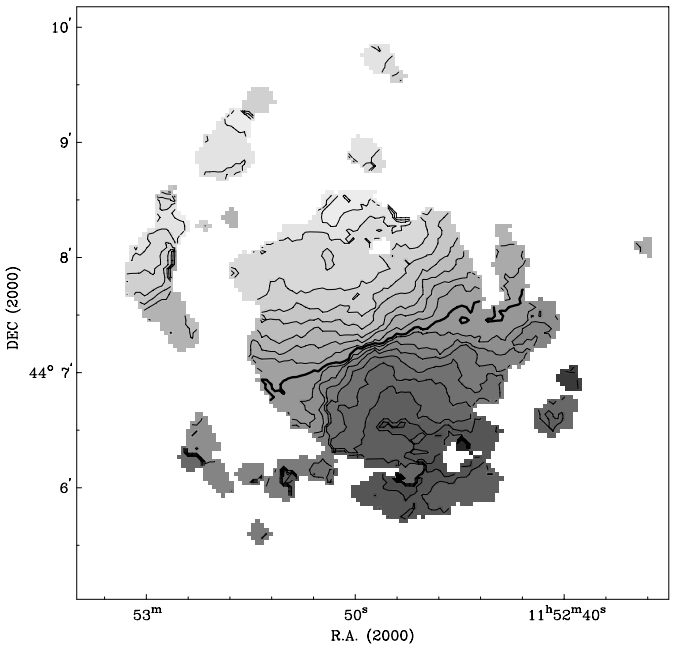

Fig. 7. Velocity map for NGC 3938 at 12 arcsec resolution. Levels are shown each 5 km s^{-1}. Dark gray shows the approaching region while light gray shows the receding region. The thick line shows the 0 km s^{-1} line.

by Norman and Ikeuchi (1989) would show this behavior, and filaments of H_α emission leaving the disk from bright HII regions have also been detected in edge on galaxies (see for example Dettmar (1990)). These chimneys are associated with the most active star forming regions as the OB associations hosted

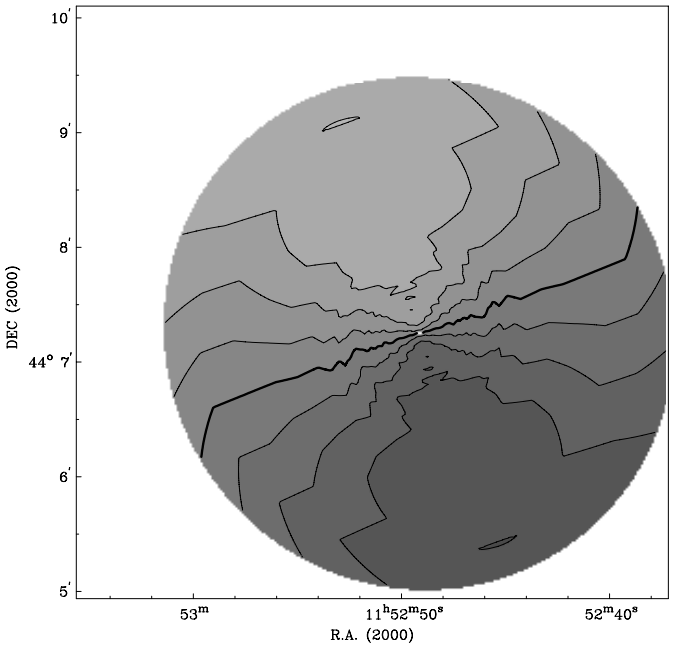

Fig. 8. Model velocity map for NGC 3938 calculated by fitting a tilted rings model to the observed velocity map. Levels are shown each 10 km s^{-1}. Dark gray shows the approaching region while light gray shows the receding region. The thick line shows the 0 km s^{-1} line.

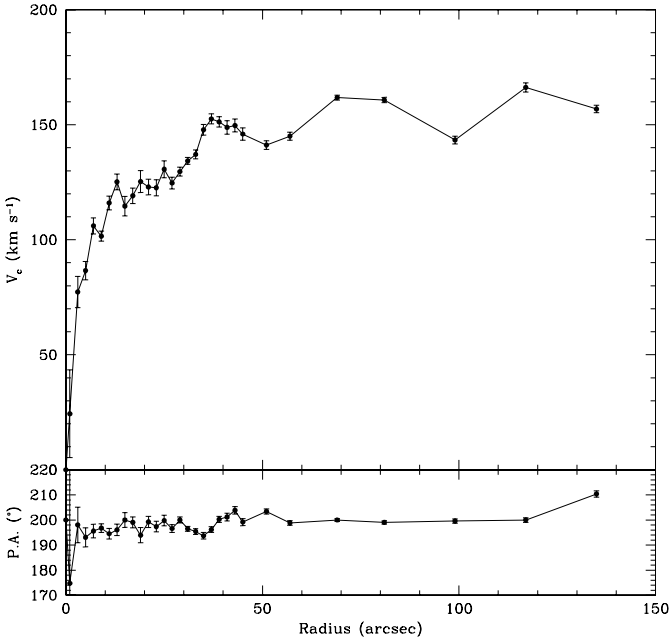

Fig. 9. Rotation curve for NGC 3938 (*upper panel*) and fitted position angle (*lower panel*). Error bars represent least-squares fit errors. The points were derived from the high resolution map but taking wider rings for the outer parts.

by supergiant HII regions, and are a very interesting possibility in understanding the disc-halo interaction in galaxies. Further observational research would be desirable to clarify this point.

5.4. The velocity dispersion map

We calculated the velocity dispersion map by the gaussian fitting method as commented upon in Sect. 3. The map is shown in Fig. 12. Some of the brightest HII regions are also visible in this map by their high velocity dispersion which goes up to 17 km s^{-1}. Anyway, there is no clear relation between intensity and velocity dispersion as we will see later. The mean velocity dispersion of the H_α emission in the whole galaxy is about 11 km s^{-1}. This value is observed to be constant within the observational errors at every galactocentric radii as shown in Fig. 13. This effect had already been found for the neutral gas by van der Kruit & Shostak (1982) and for the molecular gas by Combes & Bequaert (1997). These latter authors discuss in their paper several possible explanations for this coincidence in the vertical velocity dispersions of the different gas phases. Moreover, they found that the velocity dispersion is higher than the value needed to maintain gravitational stability. Stellar formation is rejected by them as the heating source because most of the HI showing this behavior is well outside the optical disc. Of course this is not the case for the ionized gas where new born stars are the most important heating mechanism, and which show a very similar value for the velocity dispersion. Therefore, some combination of several heating mechanisms could be acting to produce the observed behavior.

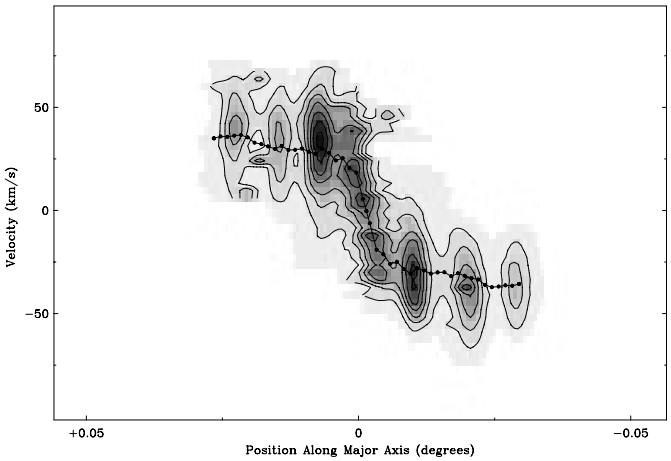

Fig. 10. Position-velocity diagram of NGC 3938 along the major axis (P. A.=20°) with the inner part of the calculated rotation curve superimposed.

6. Intensity versus velocity dispersion

We have studied the relation between velocity dispersion and intensity in NGC 3938. In this purpose we have constructed the two-dimensional distribution shown in Fig. 14 where we show the velocity dispersion (uncorrected) vs intensity for each pixel. We are aware that the region of low dispersions (below the instrumental width) in the histogram is not fully reliable, but we include it for completeness. We have calculated the mean dispersion at a given intensity (shown with the solid line in Fig. 14). The mean dispersion grows in average as $\sigma \propto I^{1/8}$, although

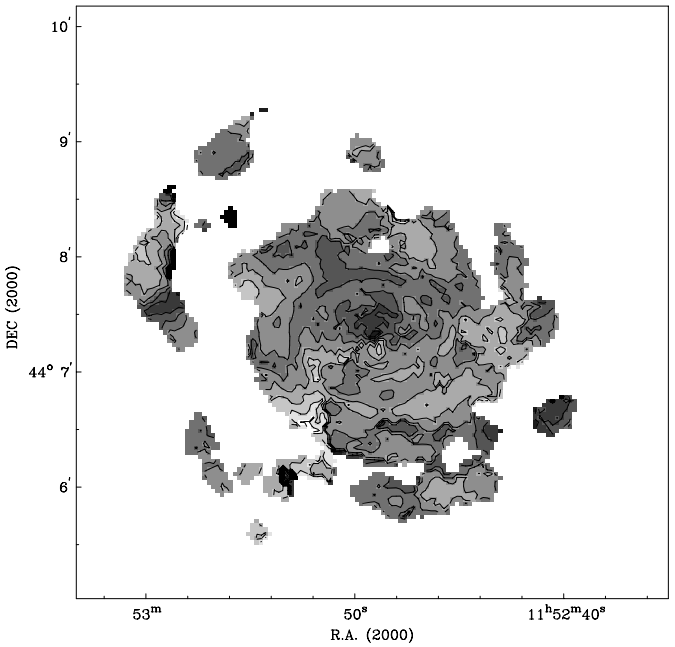

Fig. 11. Residual velocity map for NGC 3938. Contour levels are between -12 and 12 km s^{-1} (from light gray to dark gray) separated by 3 km/sec each.

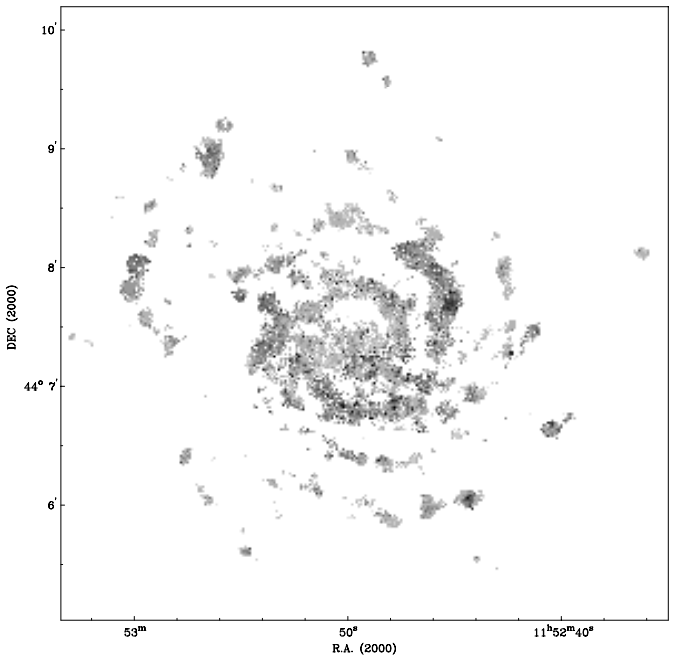

Fig. 12. Velocity dispersion map at 1.12 arcsec/pixel resolution. Gray levels range from 0 to 20 km s^{-1} (from light gray to dark gray).

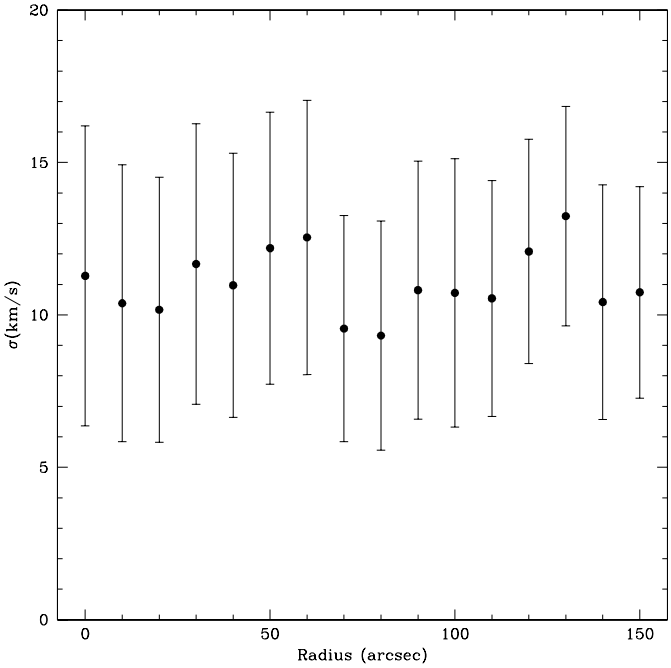

Fig. 13. Radial distribution of velocity dispersion in rings of width 11 arcsec. The data have been corrected for instrumental, natural and thermal broadening.

it becomes much flatter for high intensities, for which the dispersion becomes almost constant at a value of about 19 km/sec. Another interesting feature is the upper envelope of the distribution shown by the dashed line. The line is a function $I \propto \sigma^3$. A relation $\mathcal{L} \propto \sigma^3$ has been previously found for HII regions (note that our distribution is built for every pixel and not for HII regions) by Roy et al. (1986). We have tested if this also happens in this galaxy, but we have not found any correlation between dispersion and luminosity in a sample of 25 HII regions of NGC 3938. Arsenault et al. (1990) studied such a correlation between luminosity and dispersion in NGC 4321 and did not find any correlation if they used the full HII regions sample, although they found a correlation if they used just the brightest HII regions. We cannot confirm nor reject such a correlation with our data.

We have tried to interpret the upper envelope in the $(I - \sigma)$ distribution in terms of Kolmogorov turbulence. In this case, energy losses per volume unit and time unit would be $\rho\sigma^3/L$, being ρ the density and L the size of the HII region. The turbulent energy production (i. e. $\partial/\partial t(1/3\rho\sigma^2)$) would be of type xQ where Q is the energy density input due to stars and x a proportionality constant with a very small value. When thermal and turbulent energies reach stationary conditions, then, if production terms are proportional for both, so must be their losses. Thermal energy density losses due to radiation would be per time unit $\sigma_{SB}T^4/L$ (where σ_{SB} is the Stefan-Boltzmann constant, and T is the temperature). Under stationary conditions one would have $x\sigma_{SB}T^4 = \sigma^3\rho$. The intensity is $I \propto \sigma_{SB}T^4l^2$ (where l is a length corresponding to the pixel size) and we would have thus $I \propto \sigma^3$. In Fig. 14 we see that the upper envelope matches this relation such that true dispersion is always larger or equal than predicted by that relation. This could be understood if violent stellar phenomena (such as strong stellar winds of SN explosions) produce very large turbulent motions which afterwards trend to relax to a stationary regime compatible with Kolmogorov turbulence. This is also partially confirmed by some HII regions showing high dispersions in their

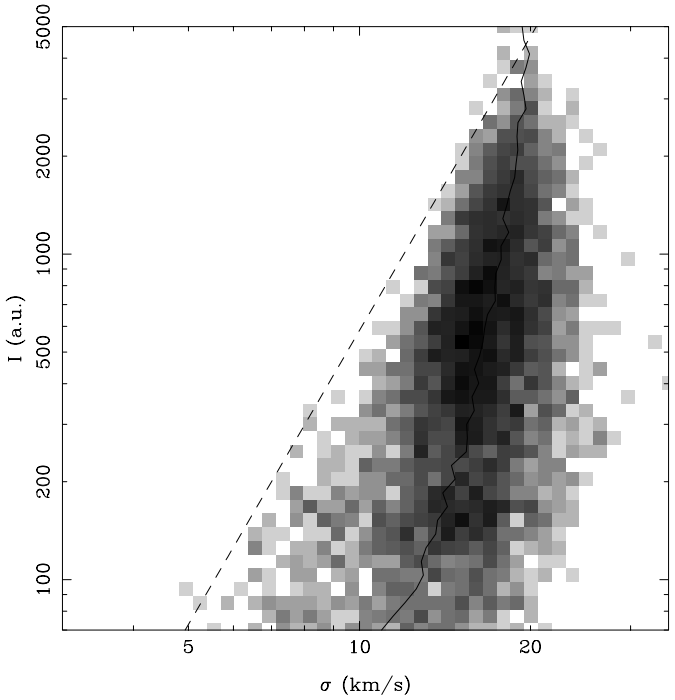

Fig. 14. Velocity dispersion vs intensity distribution. Solid line represents the mean dispersion at each intensity. Dashed line represents a function $I \propto \sigma^3$ as the upper envelope.

outer envelopes which suggest expansive motions which could have been produced by shocks resulting from SN explosions or strong stellar winds inside them.

There is an interesting case which is the previously commented supergiant HII region (northward of the pair to the east) with a systematic defect in the residual velocity. Its outer shell shows a large velocity dispersion (even larger than in the center of the HII region) with low intensity. This could be interpreted as an expanding shell. In this case the outer shell high velocity dispersion could be interpreted in terms of high temperature (of about $5 \times 10^4\,K$) due to shock heating. Anyway we warn that our spatial resolution is at the limit to detect this feature, and therefore higher spatial and spectral resolution observations could clarify this point.

7. Results and conclusions

We have studied the distribution and kinematics of the ionized gas in the spiral galaxy NGC 3938 from Fabry-Perot observations. Our main results and conclusions are:

– The velocity map of the galaxy is compatible with pure axisymmetric rotation. There are no traces of a warp and very small traces of streaming motions across the spiral arms.
– The rotation curve of the galaxy shows a standard shape with an asymptotic rotation velocity of about 157 km s^{-1} (for an inclination angle of $14°$). The rotation curve is compatible with previous determinations with HI and molecular gas observations, but we are able to determine it with much better spatial resolution in the inner 2 arcmin of the galaxy.
– The velocity dispersion of the ionized gas is kept constant with galactocentric radius at a value of about 11 km s^{-1}. This value is similar (although slightly higher) to previously reported values for the neutral and molecular gas in this galaxy. Also we find that there is no radial dependence of the vertical velocity dispersion.
– We find that the velocity dispersion vs intensity distribution has an upper envelope of the type $I \propto \sigma^3$, compatible with a Kolmogorov turbulence regime as the stationary regime. The average intensity vs velocity dispersion relation is much steeper with a mean behavior of the type $I \propto \sigma^8$ or even steeper for higher intensities, for which the dispersion is kept almost constant at a value of about 19 km s^{-1}.

Acknowledgements. We are very grateful to the referee Dr. M. Marcelin for his valuable comments and remarks on this paper. This paper has been supported by the spanish "Ministerio de Educación y Cultura" (PB96-1428) and the "Plan Andaluz de Investigación" (FQM-0108).

References

Amram P., Balkowski C., Boulesteix J., et al., 1996, A&A 310, 737
Arsenault R., Roy J-R., Boulesteix J., 1990, A&A 234, 23
Begeman K., 1989, A&A 223, 47
Bottema R., 1988, A&A 197, 105
Bottema R., 1993, A&A 275, 16
Combes F., Becquaert J-F., 1997, A&A 326, 554
Dettmar R.-J., 1990, A&A 232, L14
Foster P.A., Nelson A.H., 1985, MNRAS 215, 555
Kennicutt R.C. Jr., Edgar B.K., Hodge P.W., 1989, ApJ 337, 761
van der Kruit P.C., Shostak G.S., 1982, A&A 105, 351
McCall M.L., Straker R.W., Uomoto A.K., 1996, AJ 112, 1096
Norman C.A., Ikeuchi S., 1989, ApJ 345, 372
Osterbrock D.E., 1989, Astrophysics of gaseous Nebulae and galactic nuclei. University Science Books, Mill Valley
Rozas M., Beckman J.E., Knapen J.H., 1996, A&A 307, 735
Roy J-R., Arsenault R., Joncas G., 1986, ApJ 300, 624
Spitzer L. Jr., 1978, Physical Processes in the Interstellar Medium. J. Wiley & Sons, New York
Tully R.B., Verheijen M.A.W., Pierce M.J., Huang J-S., Wainscoat R.J., 1996, AJ 112, 2471